Quaternionic Weber Local Descriptor of Color Images

Rushi Lan, Yicong Zhou, *Senior Member, IEEE*, and Yuan Yan Tang, *Fellow, IEEE*

Abstract— This paper proposes a simple but effective framework named *quaternionic Weber local descriptor (QWLD)* for color image feature extraction. Integrating quaternionic representation (QR) of the color image and Weber's law (WL), QWLD possesses both their superiorities. It uses QR to handle all color channels of the image in a holistic way while preserving their relations, and applies WL to ensure that the derived descriptors are robust and discriminative. Using the QWLD framework, we further develop the *quaternionic-increment-based Weber descriptor* and *quaternionic-distance-based Weber descriptor* in terms of different perspectives. Extensive experiments on different color image recognition problems demonstrate that the proposed framework and descriptors outperform state-of-the-art local descriptors.

Index Terms— Color image descriptor, local feature, quaternionic representation (QR), Weber's law (WL).

I. INTRODUCTION

RECENTLY, the quaternion number system [1] has aroused a great deal of research interest in the field of color image processing [2]–[5]. A quaternion consists of one real and three imaginary parts, and the imaginary parts are usually applied to encode three components of a color image. In this paper, we call this coding strategy as *quaternionic representation (QR)* of color images. There are two main advantages of color image processing using QR. First, we can handle all color components of these images in a holistic way and consider the relations among the components; Second, quaternion algebra is a mature discipline that has a plenty of theories and tools for image processing. Therefore, QR has been involved into many applications in color images and 4-D signal processing [6]–[11].

Due to the superiorities of QR, a lot of attention has been paid to extracting features for color images using QR. These features are hand-crafted representations of color images. Generally speaking, the existing QR-based feature extraction methods can be classified into two types: global descriptors and local descriptors.

It is intuitive to extend complex-number-based descriptors to their corresponding quaternionic versions to derive features from color images. Several global quaternionic descriptors have been developed based on this idea. The proposed descriptors include the quaternionic Zernike moment descriptors [12], [13], quaternionic Fourier–Mellin moment [14] and its orthogonal version [15], quaternion pseudo-Zernike moment [15], geometric Fourier descriptor [16], hypercomplex polar Fourier descriptor [17], and quaternion moment descriptors [18]. These descriptors achieve satisfying performance in classifying the objects under similar transformations (rotation, scaling, and translation). However, if images contain more complicated changes (large pose or illumination variations), these global descriptors do not work well any more.

In order to derive more robust and discriminative descriptors, local information of the image is considered. Many local descriptors [19]–[25] have been developed for grayscale and color images. It is difficult to directly extend them in the quaternionic domain. The reason lies in that the arithmetics of quaternions are different from those of real numbers. Thus, designing complicated local descriptors in quaternionic domain is a tough task. It is more realistic to develop some simple local descriptors using QR.

The well-known local binary pattern (LBP) has been extended to the quaternionic domain [26]. A descriptor named quaternionic LBP (QLBP) was developed. To perform the LBP coding, QR is first Clifford translated [27] by one unit quaternion. This operation may cause the following problems. First, it is difficult a find a suitable quaternion for all color images. Second, this is a global operation to QR so that some local characteristics will be ignored. From this point, QLBP is not a totally local descriptor.

Meanwhile, several local descriptors have been proposed using Weber's law (WL) [28] that describes the ratio between the increment and initial intensity of a stimulus in the human visual system. WL is able to measure the local variation of the image contents in a relative manner. Numerous research results have shown that the derived descriptors are robust to different variations and show good discriminative abilities [29]–[31]. However, for a color image, these types of descriptors are usually extracted from its grayscale version or from each color channel individually. They illustrate the local characteristics of the color image without considering the relations between color channels.

TABLE I

SUMMARY OF ABBREVIATIONS AND SYMBOLS USED IN THIS PAPER

Abbr.	Symbol	Description
QR	$\dot{q}$ or $\dot{Q}$	Quaternionic representation
WL	-	Weber's law
QD	D_l	Quaternionic distance
ROQ	$\text{ROQ}(\cdot, \cdot)$	Rotation of quaternion
CTQ	$\text{CTQ}(\cdot, \cdot)$	Clifford translation of quaternion
QWLD	$\Theta(\cdot)$	Quaternionic Weber local descriptor
-	$\Phi(\cdot)$	Differential feature of QWLD
-	$\Psi(\cdot)$	Orientation feature of QWLD
QIWD	$\Phi_1(\cdot)$ and $\Psi_1(\cdot)$	Quaternionic increment based Weber descriptor
QDWD	$\Phi_2(\cdot)$ and $\Psi_2(\cdot)$	Quaternionic distance based Weber descriptor

TABLE II

BASIC PROPERTIES OF THE QUATERNION

Property	Description
Conjugate	$\dot{q}^* = a - (ib + jc + kd)$
Pure Quaternion	$\dot{q} = ib + jc + kd$
Modulus	$\|\dot{q}\| = \sqrt{\dot{q}\dot{q}^*} = \sqrt{\dot{q}^*\dot{q}}$
Unit quaternion	$\|\dot{q}\| = 1$
Inverse	$\dot{q}^{-1} = \frac{\dot{q}^*}{\|\dot{q}\|^2}$ so that $\dot{q}\dot{q}^{-1} = 1$
Modulus of multiplication	$\|\dot{q}_1\dot{q}_2\| = \|\dot{q}_1\|\|\dot{q}_2\|$

In this paper, a novel framework called *quaternionic Weber local descriptor (QWLD)* is proposed for color image feature extraction. QWLD applies WL in the quaternionic domain such that the derived descriptors absorb both advantages of WL and QR. To show how to derive new descriptors using the QWLD framework, two descriptors, namely, *quaternionic-increment-based Weber descriptor (QIWD)* and *quaternionic-distance-based Weber descriptor (QDWD)*, are proposed as examples. They are based on different strategies to describe the increment and intensity of WL in the quaternionic domain. Experiments are carried out to evaluate the proposed descriptors by different applications, and comparison results show their effectiveness.

In summary, our main contributions are listed as follows.

1) We propose the QWLD framework for color image feature extraction. To the best of our knowledge, this is the first time to derive local descriptors using WL in the quaternionic domain for color images.

2) We further develop two novel descriptors, QIWD and QDWD, as examples derived from the QWLD framework. They are derived by considering WL from different perspectives and studied theoretically and experimentally.

3) We conduct a number of experiments on different color image recognition problems to evaluate the performances of the proposed descriptors by comparing with several state-of-the-art local descriptors.

The rest of this paper is organized as follows. Section II introduces some related preliminaries. Section III presents the proposed QWLD framework. Sections IV and V describe two novel local descriptors based on the QWLD framework. Sections VI and VII give the experimental results and evaluations of the proposed descriptors. Section VIII gives the conclusion.

II. PRELIMINARIES

In this section, the related preliminary knowledge, including the quaternion algebra, existing quaternionic distances (QDs), and WL, will be given briefly. For easy reading, Table I lists the relevant abbreviations and symbols used in this paper.

A. Quaternion Algebra

A quaternion $\dot{q} \in \mathbb{H}$ consists of one real part and three imaginary parts as follows:

$$\dot{q} = a + ib + jc + kd \qquad (1)$$

where a is the real part of $\dot{q}$ and $\{ib, jc, kd\}$ are the imaginary parts, and $a, b, c, d \in \Re$ and i, j, and k are complex operators.

Let $S(\dot{q}) = a$ and $V(\dot{q}) = ib + jc + kd$. Except for the algebraic version in (1), $\dot{q}$ can be represented in the polar form as follows:

$$\dot{q} = |\dot{q}|e^{\dot{\mu}\theta} = |\dot{q}|(\cos\theta + \dot{\mu}\sin\theta) \qquad (2)$$

where $\dot{\mu} = (V(\dot{q})/|V(\dot{q})|)$ and $\theta = \tan^{-1}(|V(\dot{q})|/S(\dot{q}))$ are known as the eigenaxis and phase (or eigenangle) of $\dot{q}$. Usually, $V(\dot{q})$ is employed to represent the color image

$$\dot{Q}(x, y) = iR(x, y) + jG(x, y) + kB(x, y) \qquad (3)$$

where $\dot{Q}(x, y)$ is QR of the color pixel located at (x, y) in an image, and $R(x, y)$, $G(x, y)$, and $B(x, y)$ are its red, green, and blue components, respectively.

Several basic properties of the quaternion are described in Table II.

Some properties can be similarly derived as the complex number system, like conjugate, modulus, and inverse of the quaternion. $\dot{q}$ is called a pure quaternion if its real part a equals 0. Note that the multiplication of two quaternions is noncommutative, namely, $\dot{q}_1\dot{q}_2 \neq \dot{q}_2\dot{q}_1$, but its modulus keeps the same, i.e., $|\dot{q}_1\dot{q}_2| = |\dot{q}_1||\dot{q}_2| = |\dot{q}_2||\dot{q}_1|$.

Based on these properties, several quaternionic operators have been proposed, such as rotation and Clifford translation. The rotation of $\dot{q}$ by a unit one $\dot{p}$, denoted by $\text{ROQ}(\dot{q}, \dot{p})$, is defined as

$$\text{ROQ}(\dot{q}, \dot{p}) = \dot{p}\dot{q}\dot{p}^*. \qquad (4)$$

Equation (4) shows that rotation of quaternion is a double action manifold of the quaternion [27]. There also exists a single-action manifold, named the Clifford translation of quaternion (CTQ). The right and left CTQs of $\dot{q}$ by $\dot{p}$ are defined by

$$\text{CTQ}_r(\dot{q}, \dot{p}) = \dot{q}\dot{p} \quad \text{and} \quad \text{CTQ}_l(\dot{q}, \dot{p}) = \dot{p}\dot{q} \qquad (5)$$

where $\dot{p}$ is a unit quaternion.

B. Review of QDs

To handle quaternions, one key step is to measure QDs. Considering two color pixels, $\dot{q}_1 = r_1i + g_1j + b_1k$ and $\dot{q}_2 = r_2i + g_2j + b_2k$, $D_t(\dot{q}_1, \dot{q}_2)$ denotes the tth type of QD of $\dot{q}_1$ and $\dot{q}_2$. Because the modulus of a quaternion is nonnegative, it is intuitive to derive the following QD:

$$D_1(\dot{q}_1, \dot{q}_2) = |\dot{q}_1 - \dot{q}_2|. \qquad (6)$$

Cai and Mitra [32] pointed out that the intensity and chromaticity components of $\dot{q}_1$ can be obtained by $(\dot{\rho}\dot{q}_1\dot{\rho}^* + \dot{\rho}^*\dot{q}_1\dot{\rho})/2$ and $(\dot{\rho}\dot{q}_1\dot{\rho}^* - \dot{\rho}^*\dot{q}_1\dot{\rho})/2$, respectively, where $\dot{\rho} = e^{(\pi/4)\dot{\mu}}$. Then the following QDs are defined:

$$D_2(\dot{q}_1, \dot{q}_2) = \frac{1}{2}|(\dot{\rho}\dot{q}_1\dot{\rho}^* + \dot{\rho}^*\dot{q}_1\dot{\rho}) - (\dot{\rho}\dot{q}_2\dot{\rho}^* + \dot{\rho}^*\dot{q}_2\dot{\rho})| \quad (7)$$

$$D_3(\dot{q}_1, \dot{q}_2) = \frac{1}{2}|(\dot{\rho}\dot{q}_1\dot{\rho}^* - \dot{\rho}^*\dot{q}_1\dot{\rho}) - (\dot{\rho}\dot{q}_2\dot{\rho}^* - \dot{\rho}^*\dot{q}_2\dot{\rho})|. \quad (8)$$

Considering the intensity and chromaticity differences together, Geng *et al.* [33] proposed the following QD:

$$D_4(\dot{q}_1, \dot{q}_2) = D_2(\dot{q}_1, \dot{q}_2) + D_3(\dot{q}_1, \dot{q}_2). \quad (9)$$

Jin and Li [34] proposed a method in which they first rotate one quaternion toward the gray line $\dot{\mu}$ and combine the result with the other quaternion, that is

$$\dot{q}_3 = \dot{q}_2 + \dot{\mu}\dot{q}_1\dot{\mu}^* = r_3 i + g_3 j + b_3 k. \quad (10)$$

If $\dot{q}_1$ and $\dot{q}_2$ are closed to each other, $\dot{q}_3$ should be close to the gray line. They then derived the following QD:

$$D_5(\dot{q}_1, \dot{q}_2) = |(r_3 - \chi)i + (g_3 - \chi)j + (b_3 - \chi)k| \quad (11)$$

where $\chi = (r_3 + g_3 + b_3)/3$. Later, Jin *et al.* [4] improved $D_5(\dot{q}_1, \dot{q}_2)$ by including the luminance as follows:

$$D_6(\dot{q}_1, \dot{q}_2) = \omega D_5(\dot{q}_1, \dot{q}_2) + (1-\omega)|I(\dot{q}_1, \dot{q}_2)| \quad (12)$$

where $I(\dot{q}_1, \dot{q}_2) = k_1(r_2 - r_1) + k_2(g_2 - g_1) + k_3(b_2 - b_1)$ is the luminance difference and ω gives the importance between the chromaticity and luminance difference. $k_i(i = 1, 2, 3)$ represents the contributions of different color channels to luminance.

A detailed analysis of these QDs is not given here because it goes beyond the scope of this paper. It needs to point out that though $D_3(\dot{q}_1, \dot{q}_2)$ and $D_5(\dot{q}_1, \dot{q}_2)$ were derived by different researchers from different perspectives, there exists the following relation:

$$D_3(\dot{q}_1, \dot{q}_2) = D_5(\dot{q}_1, \dot{q}_2). \quad (13)$$

The proof of (13) is given in the Appendix.

C. Weber's Law

WL was proposed by the experimental psychologist E. Weber in the 19th century. It shows that the ratio of increment threshold in a stimulus (ΔI) to the initial stimulus intensity (I) is a constant, which can be expressed as follows:

$$\frac{\Delta I}{I} = \vartheta \quad (14)$$

where ϑ is a constant and is called the *Weber fraction*. Equation (14) also implies that the stimulus can be perceived in a relative way but not the absolute increment. A small ϑ indicates that a small percentage change in intensity is discriminable, while a large one means that a large degree change in intensity is required.

III. QWLD Framework

This section presents the proposed QWLD framework in detail. Based on this framework, two novel descriptors will be introduced as implementation examples of QWLD.
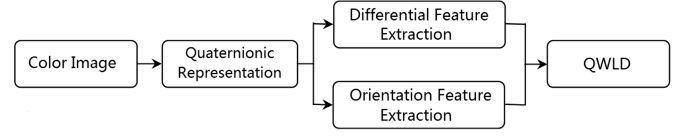

Fig. 1. QWLD framework.

A. QWLD Framework

The underlying fundamental of QWLD is to apply WL in the quaternion domain to derive the local descriptor for a color image. Fig. 1 shows the framework of QWLD. QWLD consists of two major components, namely, the differential feature and orientation feature. They are extracted from QR of a color image.

In (14), the key step of QWLD is to calculate the increment in QR of the color image. Let $\dot{q}_c$ be the center quaternion in a local patch within a color image, and $\dot{q}_l, l \in L$ denotes the rest quaternions in the patch, where L is the index set. We use $\Theta(\dot{q}_c)$ to denote the QWLD feature of $\dot{q}_c$, and it can be achieved as follows:

$$\Theta(\dot{q}_c) = \Phi(\dot{q}_c) \odot \Psi(\dot{q}_c) \quad (15)$$

where $\Phi(\dot{q}_c)$ and $\Psi(\dot{q}_c)$ are the differential and orientation features of $\dot{q}_c$, respectively, and $\odot$ is an operator to fuse two features.

1) Differential Feature: $\Phi(\dot{q}_c)$ is directly derived from WL in (14) and is represented as follows:

$$\Phi(\dot{q}_c) = \frac{\sum_{l \in L} F(\dot{q}_c, \dot{q}_l)}{\Gamma(\dot{q}_c)} \quad (16)$$

where $F(\dot{q}_c, \dot{q}_l)$ is the quaternionic increment between $\dot{q}_c$ and $\dot{q}_l$ and $\Gamma(\dot{q}_c)$ denotes the quaternionic intensity of $\dot{q}_c$. Unlike the spatial-domain increment of the grayscale image that is directly calculated using pixel values, in the quaternionic domain, we need to find a proper function to denote the *illumination* increment of quaternions and a function to represent the intensity of a quaternion. Note that (16) considers the relationship between the center pixel and all its surrounding ones.

2) Orientation Feature: Orientation information, like the edge, contains rich characteristics of images. To make the derived feature more robust, QWLD also considers the orientation feature. Let $L_1 \subset L$ and $L_2 \subset L$ be two subsets of L. The elements in L_1 and those in L_2 are distributed in different orientations within the local region. Then the orientation feature of QWLD $\Psi(\dot{q}_c)$ is defined as

$$\Psi(\dot{q}_c) = \frac{\sum_{l \in L_1} F(\dot{q}_c, \dot{q}_l)}{\sum_{l \in L_2} F(\dot{q}_c, \dot{q}_l)} \quad (17)$$

where $F(\dot{q}_c, \dot{q}_l)$ has the same meaning as in (16). L_1 and L_2 are two different subsets of L with a small overlapping such that more contrast characteristics of the local region can be extracted. For instance, L_1 contains the points in the horizontal direction, while L_2 consists of the points in the vertical direction. Note that it is possible to derive $\Phi(\dot{q}_c)$ and $\Psi(\dot{q}_c)$ using different $F(\dot{q}_c, \dot{q}_l)$.

3) Feature Fusion: $\Phi(\dot{q}_c)$ and $\Psi(\dot{q}_c)$ represent two different characteristics of color images in the quaternionic domain. A fusion step is necessary to strengthen their discriminative abilities before recognition. There exist many methods to fuse $\Phi(\dot{q}_c)$ and $\Psi(\dot{q}_c)$. One simple way is to concatenate two feature vectors together to obtain a new vector, namely, $\Theta(\dot{q}_c) = [\Phi(\dot{q}_c); \Psi(\dot{q}_c)]$. Other methods like 2-D histogram can also be used.

The QWLD framework in Fig. 1 shows the main skeleton of extracting QWLD features. WL regards the relative color contrast as local features that are robust and discriminative characteristics of the color image. Meanwhile, QR ensures that all color information is taken into account in the color contrast extraction procedure. QWLD combines QR and WL and takes both their advantages. Using the framework, we are able to derive different QWLD features by considering various types of quaternionic increments.

B. Two Implementation Examples

For QR of a color image, we need to develop proper $F(\dot{q}_c, \dot{q}_i)$ and $\Gamma(\dot{q}_c)$ for QWLD. Using different $F(\dot{q}_c, \dot{q}_i)$ and $\Gamma(\dot{q}_c)$ allows us to represent different characteristics of the color image. As examples, we apply two strategies to propose QWLDs of the color image from different perspectives.

1) *QIWD:* It is intuitive to consider the increment in the quaternionic domain directly. Based on this idea and WL, we propose QIWD.
2) *QDWD:* QDs discussed in Section II-B were proposed from different viewpoints to measure the similarity between two quaternions. They are also considered as the increments between two quaternions. Applying them to the QWLD framework, we propose QDWD.

QIWD directly implements WL in the quaternionic domain. The quaternionic operations provide a new understanding to local descriptor extraction. On the other hand, QDWD applies QDs to WL framework. These QDs are developed to detect the outliers in color images. They describe the essential relation between pixels and will benefit to QDWD for feature extraction. Next, we present these two QWLDs in detail in the following sections.

IV. QUATERNIONIC-INCREMENT-BASED WEBER DESCRIPTOR

As aforementioned, QIWD calculates the increment directly in the quaternionic domain. In this section, we will detail the derivation of QIWD. Consider a 3×3 local patch in a color image with QR as follows:

$$\begin{bmatrix} \dot{q}_0 & \dot{q}_1 & \dot{q}_2 \\ \dot{q}_7 & \dot{q}_c & \dot{q}_3 \\ \dot{q}_6 & \dot{q}_5 & \dot{q}_4 \end{bmatrix} \tag{18}$$

where $\dot{q}_c$ is the center pixel and $\dot{q}_l$ ($l \in L = \{0, \ldots, 7\}$) are surrounding ones. Denote the differential and orientation features of QIWD for $\dot{q}_c$ by $\Phi_1(\dot{q}_c)$ and $\Psi_1(\dot{q}_c)$, respectively.

A. Differential Feature

To obtain $\Phi_1(\dot{q}_c)$, we need to obtain the increment first. Based on QR, we use $\Delta \dot{I}$ to denote the increment and $\dot{I}$ to represent the initial stimulus intensity. Then $\Delta \dot{I}$ can be achieved as follows:

$$\Delta \dot{I} = \sum_{l=0}^{l=7} \Delta \dot{q}_l = \sum_{l=0}^{l=7} (\dot{q}_l - \dot{q}_c). \tag{19}$$

In this situation, we have $\dot{I} = \dot{q}_c$. However, we cannot directly calculate $(\Delta \dot{I} / \dot{I})$ as shown in (14) because there is no division operation for quaternions. To address this problem, we apply the inverse to replace $\dot{I}$ in the denominator. Due to the noncommutativity of multiplication for quaternion, it has the following:

$$\dot{I}^{-1} \Delta \dot{I} \neq \Delta \dot{I} \dot{I}^{-1} \tag{20}$$

where $\dot{I}^{-1}$ is the inverse of $\dot{I}$.

To clearly understand (20), we analyze $\Delta \dot{I}$ and $\dot{I}^{-1}$ by considering the color space. Based on the notations used in (3) and (18), the center pixel in the local patch and its surrounding ones are denoted by $\dot{q}_c = iR_c + jG_c + kB_c$ and $\dot{q}_l = iR_l + jG_l + kB_l, l = 0, 1, \ldots, 7$. Then (19) turns to

$$\begin{aligned} \Delta \dot{I} &= \sum_{l=0}^{l=7} (\dot{q}_l - \dot{q}_c) \\ &= \sum_{l=0}^{l=7} [(iR_l + jG_l + kB_l) - (iR_c + jG_c + kB_c)] \\ &= \sum_{l=0}^{l=7} [i(R_l - R_c) + j(G_l - G_c) + k(B_l - B_c)] \\ &= i\Upsilon_R + j\Upsilon_G + k\Upsilon_B \end{aligned} \tag{21}$$

where $\Upsilon_R = \sum_{l=0}^{l=7}(R_l - R_c)$, $\Upsilon_G = \sum_{l=0}^{l=7}(G_l - G_c)$, and $\Upsilon_B = \sum_{l=0}^{l=7}(B_l - B_c)$. Observing the above equation, we can find that it captures all intensity differences between the center pixel and its surrounding ones in all color channels at the same time.

To $\dot{I}^{-1}$, using the definition of the quaternion's inverse, it has the following:

$$\dot{I}^{-1} = -\frac{iR_c + jG_c + kB_c}{R_c^2 + G_c^2 + B_c^2} = -\frac{iR_c + jG_c + kB_c}{|\dot{q}_c|^2}. \tag{22}$$

Equation (22) indicates that there are two changes to $\dot{q}_c$ when considering its inverse. First, the direction of $\dot{q}_c$ in the color space turns to its opposite way. Second, the modulus of $\dot{q}_c$ is modulated. Note that this modulation is not the same as the unitization of $\dot{q}_c$.

By considering (21) and (22) together, we can obtain the following result:

$$\begin{aligned} \dot{I}^{-1} \Delta \dot{I} &= -\frac{(iR_c + jG_c + kB_c)(i\Upsilon_R + j\Upsilon_G + k\Upsilon_B)}{|\dot{q}_c|^2} \\ &= \frac{-1}{|\dot{q}_c|^2} [-(R_c\Upsilon_R + G_c\Upsilon_G + B_c\Upsilon_B) \\ &\quad + i(G_c\Upsilon_B - B_c\Upsilon_G) + j(B_c\Upsilon_R - R_c\Upsilon_B) \\ &\quad + k(R_c\Upsilon_G - G_c\Upsilon_R)]. \end{aligned} \tag{23}$$

$\Delta \dot{i} \dot{i}^{-1}$ can similarly be calculated, and they have the following relation:

$$i^{-1} \Delta \dot{i} = (\Delta \dot{i} \dot{i}^{-1})^*. \tag{24}$$

It is not difficult to find that the phases of a quaternion and its conjugate one are the same, namely

$$\theta_{\dot{i}^{-1} \Delta \dot{i}} = \theta_{\Delta \dot{i} \dot{i}^{-1}}. \tag{25}$$

On the other hand, we can understand $\dot{i}^{-1} \Delta \dot{i}$ in the following perspective:

$$\dot{i}^{-1} \Delta \dot{i} = \dot{q}_c^{-1} \sum_{l=0}^{l=7} (\dot{q}_l - \dot{q}_c) = \sum_{l=0}^{l=7} (\dot{q}_c^{-1} \dot{q}_l - 1). \tag{26}$$

In the above equation, $\dot{i}^{-1} \Delta \dot{i}$ consists of two parts: $\dot{q}_c^{-1} \dot{q}_l$ and a real number 1. The real number can be regarded as a modulation of the real part of $\dot{q}_c^{-1} \dot{q}_l$. Note that the real part directly relates to the phase of a quaternion. In order to flexibly modulate the real and imaginary parts in (26), we generalize it into the following form:

$$\widehat{\dot{i}^{-1} \Delta \dot{i}}_\alpha = \sum_{l=0}^{l=7} (\dot{q}_c^{-1} \dot{q}_l - \alpha). \tag{27}$$

Note that even if we introduce a parameter α in (27), it still has the following:

$$\theta_{\widehat{\dot{i}^{-1} \Delta \dot{i}}_\alpha} = \theta_{\widehat{\Delta \dot{i} \dot{i}^{-1}}_\alpha}. \tag{28}$$

In this work, the phase of $\theta_{\widehat{\dot{i}^{-1} \Delta \dot{i}}_\alpha}$ is used as the differential excitation of $\dot{q}_c$ as follows:

$$\Phi_1(\dot{q}_c) = \theta_{\widehat{\dot{i}^{-1} \Delta \dot{i}}_\alpha}. \tag{29}$$

In practice, $\Phi_1(\dot{q}_c)$ can be efficiently calculated. If we compute (21) in a pixel-wise way, the computation cost will be large. It can also be achieved by performing the 2-D convolution of the quaternionic matrix $\dot{Q}$ and the following matrix:

$$\begin{bmatrix} 1 & 1 & 1 \\ 1 & -8 & 1 \\ 1 & 1 & 1 \end{bmatrix}. \tag{30}$$

After that, the rest calculations for $\Phi_1(\dot{q}_c)$ (like the inverse, modulation, and phase) can be calculated by the matrix operation.

Take the color image shown in Fig. 2(a) as an example. Its differential features of QIWD are shown in Fig. 2(b)–(e). The parameter α here is set to 0.95, 1, 1.05, and 1.1, respectively. We can observe that there is still a shape of the human body in each image. α strongly affects the extracted feature. Different characteristics can be emphasized by setting with variant α values.

B. Orientation Feature

For the sake of convenience, the difference of points on the same line is used as the orientation feature. Based on a local region given in (18), this difference, denoted by ΔO_m, can be achieved as follows:

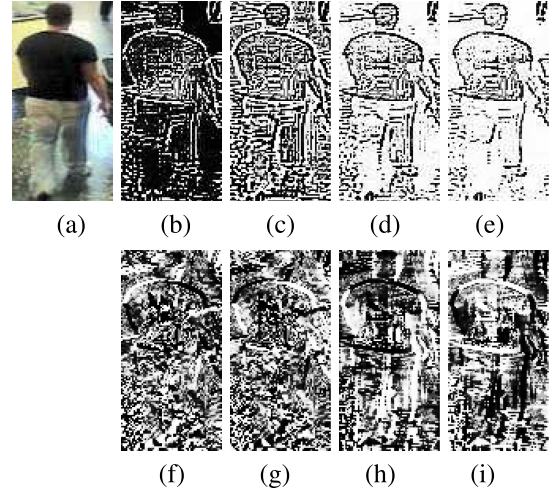$$\Delta O_m = \dot{q}_{m+4} - \dot{q}_m \tag{31}$$

Fig. 2. Image and its QIWD features. (a) Original color image. (b)–(e) Differential features of QIWD by setting α to 0.95, 1, 1.05, and 1.1, respectively. (f)–(i) Orientation features of QIWD obtained by different matrix pairs.

where $m = 0, 1, 2, 3$. As shown in (17), the ratio of two orientation differences, ΔO_m and ΔO_n ($m \neq n$), is considered. Similar to the proposed differential excitation, we apply $\Delta O_m \Delta O_n^{-1}$ or $\Delta O_n^{-1} \Delta O_m$ to replace the ratio of two quaternions. They have the following relation too:

$$\theta_{\Delta O_m \Delta O_n^{-1}} = \theta_{\Delta O_n^{-1} \Delta O_m}. \tag{32}$$

Therefore, we develop the orientation feature of $\dot{q}_c$ as follows:

$$\Psi_1(\dot{q}_c) = \theta_{\Delta O_m \Delta O_n^{-1}}. \tag{33}$$

By setting m and n to different values, we can achieve different orientation features of $\dot{q}_c$.

Note that there are several different combinations of m and n in (33). If m and n are set with two adjacent integers ($|m-n| = 1$), $\Delta O_m \Delta O_n^{-1}$ may close to 1 in most situations. In order to extract more robust orientation features, we set m and n on the condition that they satisfy $|m-n| = 2$. That is to say, the points on two orthogonal lines are considered to propose the orientation characteristics for QIWD.

As the differential excitation extraction, the orientation feature can be achieved efficiently too. Denote the following matrices by ϖ_m, $m = 0, \ldots, 3$, respectively:

$$\begin{bmatrix} -1 & 0 & 0 \\ 0 & 0 & 0 \\ 0 & 0 & 1 \end{bmatrix}, \begin{bmatrix} 0 & -1 & 0 \\ 0 & 0 & 0 \\ 0 & 1 & 0 \end{bmatrix}, \begin{bmatrix} 0 & 0 & -1 \\ 0 & 0 & 0 \\ 1 & 0 & 0 \end{bmatrix}$$
$$\begin{bmatrix} 0 & 0 & 0 \\ 1 & 0 & -1 \\ 0 & 0 & 0 \end{bmatrix}. \tag{34}$$

ϖ_0 and ϖ_2 capture the differences in the diagonal directions, and ϖ_1 and ϖ_3 represent the differences in the vertical and horizontal orientations, respectively. Then ΔO_m can be obtained by convoluting the QR of the color image with corresponding ϖ_m. The rest operations will be quickly implemented in the matrix way.

$$\theta_{\dot{i}^{-1}\Delta\dot{i}} = \tan^{-1}\frac{\sqrt{(G_c\Upsilon_B - B_c\Upsilon_G)^2 + (B_c\Upsilon_R - R_c\Upsilon_B)^2 + (R_c\Upsilon_G - G_c\Upsilon_R)^2}}{-(R_c\Upsilon_R + G_c\Upsilon_G + B_c\Upsilon_B)} \qquad (38)$$

Similarly, the orientation features of QIWD for Fig. 2(a) are shown here. As aforementioned, $\Psi(\dot{q}_c)$ considers the relationship of differences in two orientations. Based on the matrices given in (34), we select the following pairs to derive $\Psi(\dot{q}_c)$: (ϖ_0, ϖ_2), $(\varpi_0, -\varpi_2)$, (ϖ_1, ϖ_3), and $(\varpi_1, -\varpi_3)$. The corresponding results are shown in Fig. 2(f)–(i). We can find that it is difficult to find the shape of the human body in Fig. 2(f) and (g), while Fig. 2(h) and (i) shows a clear shape of the human body.

C. Discussion

Here, we discuss the proposed QIWD from different perspectives. First, QIWD needs to calculate the multiplication between a quaternion and the inverse of another one in the derivation of QIWD (like $\dot{i}^{-1}\Delta\dot{i}$ and $\Delta O_m \Delta O_n^{-1}$). Note that this multiplication is not equivalent to CTQ in most cases.[1] Performing CTQ on two different quaternions, $\dot{q}_m$ and $\dot{q}_n$, with a unit quaternion $\dot{p}$, we have

$$|\dot{p}\dot{q}_m - \dot{p}\dot{q}_n| = |\dot{p}||\dot{q}_m - \dot{q}_n| = |\dot{q}_m - \dot{q}_n|. \qquad (35)$$

Thus, CTQ keeps the distance between quaternions.

If $\dot{p}$ is a pure and nonunit quaternion, its inverse is as follows:

$$\dot{p}^{-1} = \frac{\dot{p}^*}{|\dot{p}|^2} = -\frac{1}{|\dot{p}|}\ddot{p} \qquad (36)$$

where $\ddot{p} = (\dot{p}/|\dot{p}|)$ is the unitization of $\dot{p}$ such that $|\ddot{p}| = 1$. In this situation, we can achieve the following result:

$$|\dot{p}^{-1}\dot{q}_m - \dot{p}^{-1}\dot{q}_n| = \frac{1}{|\dot{p}|}|\dot{q}_m - \dot{q}_n|. \qquad (37)$$

Comparing with (35), (37) contains a coefficient $(1/|\dot{p}|)$. If $\dot{p}$ is a nonunit quaternion set to different values, the results of (37) will differ.

In [26], a descriptor named quaternionic LBP was proposed. QLBP performs CTQ on the QR of the color image with a quaternion such that all points are translated in a whole way in the quaternionic space. Considering QIWD, as shown in (37), the used multiplication scales the distance between quaternions, and the degree of scaling is determined by the modulus of the center pixel. Therefore, QIWD is adaptive and represents local characteristics.

On the other hand, the phase of the multiplication of two quaternions is used for QIWD. Considering the phase of $\dot{i}^{-1}\Delta\dot{i}$ in (23), it has (38), as shown at the top of this page.

Equation (38) does not simply consider the ratio of the increment to the initial intensity as shown in (14). It actually describes the similarity of two vectors, namely, the intensity of center pixel $(R_c, G_c, B_c)^T$ and its total difference with surrounding ones $(\Upsilon_R, \Upsilon_G, \Upsilon_B)^T$. In (38), the denominator

is the inner product of these two vectors, while the numerator is the total difference of all two color components. If the two vectors are closed to each other, the value of $\theta_{\dot{i}^{-1}\Delta\dot{i}}$ will be large. The parameter α used in (27) will influence the denominator of (38), which is applied to modulate the correlation and difference of the two vectors.

Similarly, the orientation feature $\theta_{\Delta O_m \Delta O_n^{-1}}$ of QIWD can also be analyzed as (38). The difference lies in that (38) illustrates the relation between $(R_c, G_c, B_c)^T$ and $(\Upsilon_R, \Upsilon_G, \Upsilon_B)^T$, while $\theta_{\Delta O_m \Delta O_n^{-1}}$ considers the relation between $(R_{m+4} - R_m, G_{m+4} - G_m, B_{m+4} - B_m)^T$ and $(R_{n+4} - R_n, G_{n+4} - G_n, B_{n+4} - B_n)^T$, which are the differences of points in two lines. As a result, $\theta_{\Delta O_m \Delta O_n^{-1}}$ considers the local feature of the color image in another perspective.

Although Weber local descriptor (WLD) and QWLD are both based on WL, QIWD includes a deeper relationship between pixels than WLD. The essential principle of the WL-based descriptor lies in that they use the local contrast between pixels as the features. WLD extracts the contract directly using the intensities of pixels, which is similar to the first-order gradient of the image. On the contrary, QIWD first calculates the total color contrasts between the central pixel and its surrounding ones $(\Upsilon_R, \Upsilon_G, \Upsilon_B)^T$, and then considers the differences between these contrasts and the center pixel $(R_c, G_c, B_c)^T$ in the form of $(G_c\Upsilon_B - B_c\Upsilon_G)$ that can be regarded as the second-order gradient of the image. Therefore, features derived by QIWD are more robust to different variations and contain more discriminative characteristics of the image.

In practice, images are usually captured in unwanted environments, like the poor light condition, occlusion, or change of the view angle. Hence, the developed local descriptor is expected to be robust against these variations. To this end, the dense local histogram is extracted from overlapping cells in the QWLD result. In this work, the centers of all these cells have a uniform distribution. The histogram contains 16 bins, and it is normalized such that its sum is 1. Finally, concatenating the normalized histograms generates the QWLD feature representation of the original color image.

V. QUATERNIONIC-DISTANCE-BASED WEBER DESCRIPTOR

In this section, we introduce the proposed QDWD in detail. The local patch in (18) is used here too. Denote the differential and orientation features of QDWD by $\Phi_2(\dot{q}_c)$ and $\Psi_2(\dot{q}_c)$, respectively.

A. QDWD

QDs measure the similarity between two quaternions. The higher similarity corresponds to a smaller distance. If two quaternions have a large distance, there must be some increment between them to reduce the similarity.

---

[1]When $|\dot{i}| = 1$, $\dot{i}^{-1}\Delta\dot{i}$ is the CTQ of $\Delta\dot{i}$ with $\dot{i}^{-1}$. $\Delta O_m \Delta O_n^{-1}$ is of the same situation.
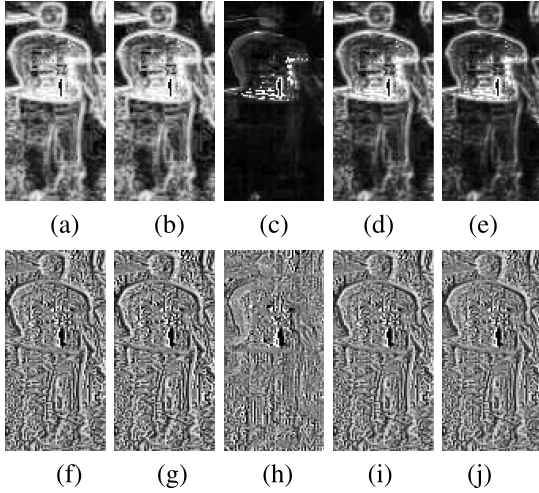
Fig. 3. QDWD features of Fig. 2(a). (a)–(e) Differential features of QDWD using different QDs. (f)–(j) Corresponding orientation features.

Therefore, it is reasonable to apply QDs to describe the quaternionic increment between quaternions. In (16), it has $F(\dot{q}_c, \dot{q}_l) = D_t(\dot{q}_c, \dot{q}_l)$ in this situation. Using different QDs, the derived QDWD will differ too. Let $\Phi_2^t(\dot{q}_c)$ denote the differential feature of QDWD derived by D_t.

Then the total quaternionic increment in this local patch can be represented as $\sum_{l=0}^{l=7} D_t(\dot{q}_l, \dot{q}_c)$. To derive $\Phi_2^t(\dot{q}_c)$, we also need to find the quaternionic intensity $\Gamma(\dot{q}_c)$ for $\dot{q}_c$ in (16). In this work, the modulus of $\dot{q}_c$, $|\dot{q}_c|$, is used as the quaternionic intensity. It is the actually Euclidean distance of $\dot{q}_c$ and the original point in the color space. Then $\Phi_2^t(\dot{q}_c)$ can be achieved as follows:

$$\Phi_2^t(\dot{q}_c) = \arctan\left(\frac{\sum_{l \in L} D_t(\dot{q}_l, \dot{q}_c)}{|\dot{q}_c|}\right). \tag{39}$$

The nonlinear mapping $\arctan(\cdot)$ is used here to make $\Phi_2^t(\dot{q}_c)$ more robust [30].

Note that in $\Phi_2^t(\dot{q}_c)$, the increments in all directions are considered. Unlike $\Phi_2^t(\dot{q}_c)$, the orientation feature of QDWD $\Psi_2(\dot{q}_c)$ aims to highlight the orientation characteristics of the local patch. Similar to the orientation feature of QIWD, we consider the relations of QDs in two orthogonal lines to derive $\Phi_2^t(\dot{q}_c)$ as follows:

$$\Psi_2^t(\dot{q}_c) = \arctan\frac{D_t(\dot{q}_{m+4}, \dot{q}_c) - D_t(\dot{q}_m, \dot{q}_c)}{D_t(\dot{q}_{n+4}, \dot{q}_c) - D_t(\dot{q}_n, \dot{q}_c)}. \tag{40}$$

The criterion to select m and n in (40) is the same as that in the orientation feature of QIWD.

Fig. 3 shows an example of QDWD features for a given color image. The image shown in Fig. 2(a) is used here. Fig. 3(a)–(e) shows the differential features of QDWD obtained using D_t, $t = 1, 2, 3, 4, 6$, respectively. Fig. 3(f)–(j) shows the corresponding orientation features by setting $m = 0$ and $n = 2$. The results obtained by the fifth QD are not shown here because they are equivalent to those of the third QD. We can observe that there is a shape of human body in each image, and the results of differential and orientation features are different. Fig. 3(a) is similar to Fig. 3(b) because they are both derived by intensity-based QDs. Fig. 3(c), obtained by

chromaticity-based QD, is different from Fig. 3(a) and (b). The results in Fig. 3(d) and (e), achieved by combining intensity and chromaticity differences, are more similar to those derived by intensity-based QDs. These images represent different characteristics of the color images and can be used for recognition.

B. Discussion

Based on the QWLD framework, we proposed QDWD for color images. QDWD applies QDs to measure the quaternionic increments. QDs are robust metrics to describe the similarity between pixels such that the derived descriptors reveal the essential relationship in a local region. QDs also represent different image characteristics from various perspectives, which offer options to design QDWD. For instance, QDWD obtained by D_2 will reflect more intensity characteristics of the color image, while QDWD with D_3 will focus on the chromaticity feature of the image. Though QDWD is able to extract the discriminate characteristics of color images, it may suffer from the limitation of large computation cost. The reason lies in that we need to rotate the quaternions and implement other operations to obtain a QD, and all the QDs between the center pixel and its surrounds ones are calculated for each local patch. This limitation will restrict the performance of QDWD.

VI. Performance Analysis of QDWD and QIWD

In this section, several experiments will be carried out to analyze the performances of the proposed QWLDs from the following perspectives. First, we study the effects of different parameter settings for QDWD and QIWD. Second, we compare the performance of these two descriptors. Third, QDWD and QIWD will be evaluated by comparing with two closely related methods, i.e., QLBP and WLD.

The person reidentification task [35], [36] is used for performance analysis in this section, which aims to classify the persons that appear in nonoverlapping visual surveillance systems. It is quite a challenging problem because it requires robust and discriminate features. The i-LIDS Multiple-Camera Tracking Scenario (MCTS) data set (119 persons and 476 images)[2] [37], [38] is selected here. Experiments are set in the following way [35]: all images of N persons are randomly chosen from the original data set to form a test set, which is further divided into two parts: a gallery set and a probe set. Note that there is one image for each person in the gallery set, and the rest images form the probe set. Two images are considered to be the same person if they have the smallest l_1-norm distance [39]. The average cumulative match characteristic (CMC) [35] is used to illustrate the ranked matching rates over 10 times of the repeated matching. A matching rate of the top rank score r means that the correct reidentification is obtained from the top r ranks with respect to N gallery images.

A. Evaluating Parameters of QIWDs

This experiment studies the performance of QIWDs that are set to different parameters. First, let us consider the differential

[2]http://www.eecs.qmul.ac.uk/~jason/

TABLE III

TOP-RANKED MATCHING RATES (IN PERCENT) OF QIWDs DERIVED BY DIFFERENT PARAMETERS ON i-LIDS MCTS ($N = 75$)

Method	$r = 1$	$r = 5$	$r = 10$	$r = 15$	$r = 20$	$r = 25$
$QIWD_{0.7,d}$	14.96	32.54	44.39	51.67	58.06	63.89
$QIWD_{0.8,d}$	17.62	35.28	46.63	54.55	61.32	66.96
$QIWD_{0.9,d}$	20.03	39.04	51.58	59.34	65.48	70.52
$QIWD_{1.0,d}$	14.15	30.11	42.24	50.71	57.99	64.56
$QIWD_{1.1,d}$	**22.26**	**41.94**	**53.49**	**61.59**	**67.44**	**72.50**
$QIWD_{1.2,d}$	20.57	39.64	51.58	59.96	66.62	71.99
$QIWD_{1.3,d}$	19.34	38.31	50.68	60.09	66.53	71.68
$QIWD_{1,o}$	17.03	37.19	49.01	57.83	64.76	**71.30**
$QIWD_{2,o}$	17.43	36.97	49.30	58.12	**65.27**	70.90
$QIWD_{3,o}$	20.34	**39.41**	50.81	58.10	64.26	69.27
$QIWD_{4,o}$	**20.70**	39.09	**51.14**	**58.52**	64.75	69.60

TABLE IV

TOP-RANKED MATCHING RATES (IN PERCENT) OF QDWDs DERIVED BY DIFFERENT QDs ON i-LIDS MCTS ($N = 75$)

Method	$r = 1$	$r = 5$	$r = 10$	$r = 15$	$r = 20$	$r = 25$
$QDWD_{1,d}$	21.38	40.58	51.40	59.68	66.00	71.21
$QDWD_{2,d}$	21.21	40.19	51.53	59.78	65.97	71.27
$QDWD_{3,d}$	20.47	39.48	49.77	57.53	64.50	69.72
$QDWD_{4,d}$	21.98	41.43	52.11	**60.35**	**66.00**	**71.72**
$QDWD_{6,d}$	**22.17**	**41.72**	**52.54**	59.63	65.67	71.09
$QDWD_{1,o_1}$	13.90	29.78	40.53	48.33	55.03	60.75
$QDWD_{2,o_1}$	14.40	29.98	40.63	48.52	55.08	61.41
$QDWD_{3,o_1}$	12.22	27.87	39.35	47.34	54.95	**61.75**
$QDWD_{4,o_1}$	**14.80**	**30.58**	40.75	**49.85**	**56.16**	61.72
$QDWD_{6,o_1}$	14.07	29.07	**41.34**	49.50	55.19	60.93
$QDWD_{1,o_2}$	14.77	30.88	43.29	51.86	57.95	64.12
$QDWD_{2,o_2}$	15.23	32.36	43.92	52.38	58.81	65.18
$QDWD_{3,o_2}$	12.85	31.44	44.03	52.61	60.29	**66.31**
$QDWD_{4,o_2}$	**15.45**	**32.74**	**44.11**	**53.36**	**60.84**	66.27
$QDWD_{6,o_2}$	13.79	32.10	43.93	52.70	59.99	65.97

feature of QIWD. As shown in (27), the parameter α is a modulation of the real and imaginary parts of (26). Denote the differential feature of QIWD with α by $QIWD_{\alpha,d}$. α is set to be $0.7, 0.8, \ldots, 1.3$ in this experiment. The experimental results are given in the first part of Table III. We can find that α greatly affects the performance of $QIWD_{\alpha,d}$. $QIWD_{1.1,d}$ obtains the most satisfying results here, while $QIWD_{1.0,d}$ performs worst. The matching rates of $QIWD_{1.1,d}$ are almost 10% higher than those of $QIWD_{1.0,d}$.

As mentioned before, the orientation feature is determined by the selection of the orientation in the local patch. Subsequently, the QR of color images is convoluted with the matrix pairs described in Section IV-B, which are combinations of those matrices in (34), to derive features. Based on the four combinations of these matrices given in Section IV-B, we denote the corresponding features by $QIWD_{t,o}$, $t = 1, \ldots, 4$, respectively. The results of all $QIWD_{t,o}$ are shown in the second part of Table III. The results indicate that the matching rates of $QIWD_{1,o}$ and $QIWD_{2,o}$ are similar. Same situations happen to $QIWD_{3,o}$ and $QIWD_{4,o}$ too. When r is set to small values ($r = 1, 5, 10$), the results of $QIWD_{3,o}$ and $QIWD_{4,o}$ are superior to those of $QIWD_{1,o}$ and $QIWD_{2,o}$, namely, the diagonal features of QIWD are more discriminative than the horizontal and vertical features. All of $QIWD_{t,o}$ perform equally if r is given larger values.

B. Evaluating QD Selection of QDWD

In this section, we study the performance of QDWDs using different QDs. As aforementioned, the derived QDWDs will differ if different QDs are selected, and the performance of QDWD closely depends on the selected QD. In Section II-B, we have introduced six QDs. Using these QDs, we can obtain six QDWD features. Denote the differential and orientation features of QDWD using the tth QD by $QDWD_{t,d}$ and $QDWD_{t,o}$. The parameters for $QDWD_{t,o}$, (m, n) in (40) are set to be $(0, 2)$ and $(1, 3)$. Denote the obtained features by $QDWD_{t,o_1}$ and $QDWD_{t,o_2}$, respectively. The person number N is set to 75 here. The top matching rates are shown in Table IV. The results of QDWD derived by the fifth QD are not given here because they are the same as those derived by the third one.

From Table IV, we can make the following key observations from the experimental results.

1) $QDWD_{t,d}$ outperforms $QDWD_{t,o}$ in all situations by about 5%–10%, which indicates that the differential features of QDWD are more discriminative than its orientation features.
2) $QDWD_{1,d}$ and $QDWD_{o,d}$ consider the Euclidean distance in the RGB color space. We can improve their performances by designing suitable distances in the quaternion domain. The features derived by the fourth QD achieve the most satisfying results among all QDs.
3) Orientation features are sensitive to the selection of direction pairs in (40). $QDWD_{t,o_2}$ gains better results than $QDWD_{t,o_1}$ in all cases.

C. QDWD Versus QIWD

In this experiment, a comparison of QDWD and QIWD is given. Since previous two experiments given in Sections VI-A and VI-B are carried out with the same settings, we can first observe Tables III and IV to compare the performances of QDWD and QIWD, respectively. Among all methods, $QIWD_{1.1,d}$ obtains the best results. Considering differential features, the results of different $QDWD_{t,d}$s are more stable than those of $QIWD_{\alpha,d}$. For orientation features, $QIWD_{t,o}$ obviously outperforms $QDWD_{t,o}$.

Differential and orientation features represent different characteristics of the original color image. Here, we apply a simple way to fuse them and use to classify. Two examples of each descriptor are constructed and evaluated here. The first example corresponds to the optimal parameter settings given in Section VI-A (or Section VI-B). The second example is randomly chosen from other possible choices. They are $QDWD\_1 = [QDWD_{3,d}; QDWD_{3,o_2}]$, $QDWD\_2 = [DQDW_{6,d}; QDWD_{6,o_2}]$, $QIWD\_1 = [QIWD_{1.1,d}; QIWD_{3,o}]$, and $QIWD\_2 = [QIWD_{1.2,d}; QIWD_{4,o}]$. The experimental results are shown in Fig. 4. We can find that different degrees of improvements can be achieved by combining differential and orientation features together. The performances of QDWD_1 and QDWD_2 are similar, while the results of QIWD_2 are about 4% higher than those of QIWD_1. In most cases, the QIWD features obtain better matching results than the QDWD features in the person reidentification task.
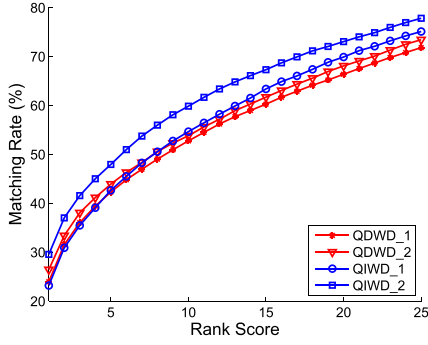
Fig. 4. CMC results of QDWD and QIWD on i-LIDS MCTS ($N = 75$).

TABLE V
TOP-RANKED MATCHING RATES (IN PERCENT) OF
QWLD AND QLBP ON i-LIDS MCTS ($N = 80$)

Method	$r = 1$	$r = 5$	$r = 10$	$r = 15$	$r = 20$	$r = 25$
$QLBP_i$	21.87	39.48	50.86	58.47	65.40	70.77
$QLBP_j$	17.03	35.28	46.85	55.13	63.08	69.06
$QLBP_k$	20.45	38.08	48.40	56.52	62.86	68.91
$QIWD_{1.1,d}$	22.53	42.60	54.87	61.88	67.78	72.70
$QIWD_{4,o}$	20.24	39.07	50.27	57.85	63.98	68.78
$QDWD_{6,d}$	22.10	41.65	51.82	58.30	64.32	69.84
$QDWD_{6,o_2}$	13.75	31.87	43.11	51.58	59.25	65.63
$QLBP_{i,j,k}$	23.54	42.71	53.87	61.60	67.89	72.89
QIWD	**28.92**	**48.16**	**59.80**	**67.32**	**72.81**	**76.90**
QDWD	25.58	44.90	54.83	61.46	67.33	72.81

D. QWLD Versus QLBP

In this experiment, QWLD is compared with another quaternionic local descriptor QLBP, which is an extension of classical LBP in the quaternionic domain. The i-LIDS MCTS data set is still used here. Performing CTQ on the QR of the color image with different unit quaternions, we can obtain several QLBP features. As for the descriptions in [26], we derive three QLBP features, denoted by $QLBP_i$, $QLBP_j$, and $QLBP_k$, by Clifford translating the image by i, j, and k, respectively. The differential and orientation of QIWD, $QIWD_{1.1,d}$ and $QIWD_{4,o}$, are selected for comparison. To QDWD, the following features are chosen: $QDWD_{6,d}$ and $QDWD_{6,o_2}$. The person number N is set to 80 here. The matching results are given in Table V. We can observe that $QIWD_{1.1,d}$ outperforms all other methods, and $QLBP_i$ works better than those of $QIWD_{4,o}$. In most cases, the matching rates of $QIWD_{3,o}$ are higher than those of $QLBP_j$ and $QLBP_k$. The results of $QDWD_{6,d}$ are comparable with those of $QLBP_i$.

We also concatenate all QLBP features together to get a new feature vector, denoted by $QLBP_{i,j,k}$. Similar operations are conducted to the corresponding QWLD features, and the derived features are denoted as QIWD = $[QIWD_{1.1,d}; QIWD_{4,o}]$ and QDWD = $[QDWD_{6,d}; QDWD_{6,o_2}]$. The matching results are also shown in Table V. $QLBP_{i,j,k}$ achieves improvements about 2%, while the improvements of QIWD are more significant than the results of a single differential or orientation feature. QIWD still keeps about 4% higher than $QLBP_{i,j,k}$ in all cases. QDWD outperforms QLBP when r is set to small values.

TABLE VI
TOP-RANKED MATCHING RATES (PERCENT) OF QWLD
AND WLD ON i-LIDS MCTS

Methods	$N = 30$					
	r=1	r=5	r=10	r=15	r=20	r=25
WLD	33.59	60.71	74.94	83.93	90.83	95.10
QDWD	35.47	59.92	73.71	83.34	90.65	95.75
QIWD	**37.54**	**64.60**	**78.23**	**86.39**	**92.70**	**97.24**
Methods	$N = 60$					
	r=1	r=5	r=10	r=15	r=20	r=25
WLD	27.67	49.59	60.86	69.21	75.20	80.63
QDWD	29.94	48.13	61.86	70.93	76.08	81.57
QIWD	**30.13**	**52.18**	**64.63**	**72.77**	**78.96**	**83.40**
Methods	$N = 90$					
	r=1	r=5	r=10	r=15	r=20	r=25
WLD	27.11	45.15	55.83	62.45	68.32	73.12
QDWD	26.49	45.36	54.64	63.03	68.06	72.03
QIWD	**28.18**	**47.23**	**57.62**	**65.31**	**70.81**	**76.02**

E. QWLD Versus WLD

Since QWLD is an extension of WLD in the quaternionic domain, a detailed comparison of them is given in this experiment using the i-LIDS MCTS data set. For the color image, the WLD features are derived by concatenating the descriptors extracted from each color channel together, namely, WLD = $[WLD_R; WLD_G; WLD_B]$. Each element in WLD contains both the differential and orientation features. To comprehensively reveal the color characteristics, two QIWD features, denoted by $QIWD_1 = [QIWD_{0.75,d}; QIWD_{1,o}]$ and $QIWD_2 = [QIWD_{1.25,d}; QIWD_{3,o}]$, are chosen to form the final descriptors for QIWD. Similarly, two QDWD features, $QDWD_4 = [QDWD_{4,d}; QDWD_{4,o_2}]$ and $QDWD_6 = [QDWD_{6,d}; QDWD_{6,o_2}]$, are concatenated together for QDWD. The person number N is set to 30, 60, and 90. The experimental results are shown in Table VI. Observing Table VI, it can be seen that WLD and QDWD achieve comparable performances in this situation. WLD outperforms QDWD when N is set to 30 and 90, while QDWD obtains better results when N is equal to 60. The matching rates of QIWD surpass those of WLD and QDWD in all cases because QIWD takes more relations among color channels into account. These results indicate that considering the interactions between color channels can improve the discriminative capacity of a descriptor.

VII. PERFORMANCE EVALUATION IN VARIOUS APPLICATIONS

In this section, experiments will be carried out to evaluate the proposed QWLD descriptors by comparing with other state-of-the-art local descriptors with different applications.

A. Experimental Data Sets

As aforementioned, local descriptors have extensive applications. In this paper, we apply the following problems for evaluation.

1) *Texture Classification:* This is one conventional application for local descriptors. The color texture data set, KTH-TIPS2-a [40] (4395 images for 11 materials), is selected here. This data set consists of four physical

planar samples of each of the 11 materials (including wood, wool, and linen). Specifically, these samples are obtained under four different illumination degrees at nine scales and three different pose changes. In this test, those texture images with a size of 200×200 are considered such that a total of 4395 texture images are used.

2) *Face Analysis:* Two face analysis tasks are selected for evaluation, namely, kinship verification and face recognition. Kinship verification is a novel face analysis problem to determine whether there is a kinship relation between face image pairs. To tackle this problem, the first step is to extract features from facial images. It is a challenging problem because there may exist great pose, illumination, and aging variations between the kinship images. Two standard data sets, KinFaceW-I (533 face image pairs) and KinFaceW-I (1000 face image pairs) [41], [42], are chosen. For face recognition, the Nanjing University of Science and Technology (NUST) real-world face recognition (RWFR) database[3] is used here. It contains 2400 face images of 100 subjects. For each person, half of the images are of high quality, while the others are captured under poor environments.

3) *Person Reidentification:* Except the i-LIDS MCTS data set, two other standard data sets are used, namely, ETHZ (146 persons and 8580 images)[4] [43] and viewpoint invariant pedestrian recognition (VIPER) (632 persons and 1246 images)[5] [44].

B. Texture Classification

Local descriptors have shown impressed performances in texture classification. In this experiment, we utilize the color texture data set, KTH-TIPS2-a [40], to evaluate QIWD and QDWD. The experiment here is conducted as in [30] and [40], namely, three images are randomly selected from the whole data set for training of each material and rest of the images are applied as the test set. The nearest neighbor classifier is used here with l_1-norm as the distance measurement between feature vectors. This experiment is repeated four times by randomly choosing the training samples, and the average value over four runs is reported here. The proposed descriptors are compared with the following approaches: QLBP [26], WLD [30], LBP [45], local color vector binary pattern (LCVBP) [46], and discriminative robust local binary pattern (DRLBP) and discriminative robust local ternary pattern (DRLTP) [47], respectively. LBP and WLD here are derived by concatenating all those descriptors extracted from each color channel together, and the rest methods are also derived by taking all color information into account. The QWLD features used in Section VI-E are selected for evaluation. The comparison results are shown in Table VII. It can be seen that QIWD achieves the most satisfying result in this situation. WLD,

TABLE VII

RECOGNITION RESULTS ON TEXTURE DATA SET KTH-TIPS2-a USING DIFFERENT METHODS

Methods	KTH-TIPS2-a Data set
LBP	58.2
WLD	61.0
LCVBP	61.5
QLBP	61.7
DRLBP	59.0
DRLTP	62.6
QDWD	60.5
QIWD	**63.4**

TABLE VIII

CLASSIFICATION ACCURACIES (IN PERCENT) OF DIFFERENT FEATURE REPRESENTATION METHODS ON TWO KinFace DATA SETS

Methods	KinFaceW-I Data Set				
	F-S	F-D	M-S	M-D	Mean
LBP	70.5	69.4	68.9	76.0	71.2
LCVBP	69.6	66.9	68.5	73.0	69.5
WLD	71.2	65.7	68.6	77.7	70.8
QLBP	69.9	67.5	68.1	75.7	70.3
QDWD	71.8	65.2	67.3	75.3	69.9
QIWD	**73.7**	**69.7**	**72.8**	**78.0**	**73.6**

Methods	KinFaceW-II Data Set				
	F-S	F-D	M-S	M-D	Mean
LBP	73.8	68.0	76.6	73.2	72.9
LCVBP	74.8	71.6	75.6	73.4	73.9
WLD	72.4	71.2	76.2	75.4	73.8
QLBP	75.2	68.6	76.8	75.6	74.1
QDWD	73.6	68.6	77.0	73.8	73.3
QIWD	**77.4**	**73.6**	**78.4**	**76.8**	**76.6**

LCVBP, and QLBP obtain similar performances, and they outperform LBP, DRLBP, and QDWD. DRLTP surpasses LCVBP and QLBP by about 1%, but it works worse than QIWD.

C. Face Analysis

1) *Kinship Verification:* As mentioned previously, two data sets, KinFaceW-I and KinFaceW-II, are employed for evaluation. Four kinship relations are considered for verification: father–son (F-S), father–daughter (F-D), mother–son (M-S), and mother–daughter (M-D). More details about the data sets can be found in [42]. The experiments here are implemented as in [42], where the neighborhood repulsed metric learning method is carried out using the proposed QWLD features to determine the relation between image pairs.

The following local descriptors are chosen for comparison in this experiment, namely, QLBP [26], WLD [30], LBP [45], and LCVBP [46]. Note that these approaches are derived by applying all color information. The results are reported in Table VIII. For the KinFaceW-I data set, QIWD outperforms other methods for all relation verification cases by different degrees, and LBP achieves the second best performance. The average classification rate of QIWD is higher than that of LBP by more than 2%. QDWD, QLBP, and LCVBP obtain similar results in this situation. Considering the KinFaceW-II data set, QLBP gains the most satisfying results among all LBP-based methods, and it works slightly better than WLD. For the WL-based schemes, QIWD acquires the best classification rates and surpasses QLBP.

TABLE IX
TOP-RANKED MATCHING RATES (IN PERCENT) ON THE NUST RWFR DATA SET

Methods	$N = 30$					$N = 60$					$N = 90$				
	$r=1$	$r=5$	$r=10$	$r=15$	$r=20$	$r=1$	$r=5$	$r=10$	$r=15$	$r=20$	$r=1$	$r=5$	$r=10$	$r=15$	$r=20$
LBP	29.64	51.74	66.59	77.61	86.12	24.01	40.78	51.86	60.20	67.07	21.85	35.97	45.02	51.75	57.18
RLBP	27.03	51.16	67.61	79.19	87.46	21.81	39.70	51.20	59.88	66.49	19.59	34.76	44.46	51.31	56.71
CLBP	27.41	50.72	65.51	75.94	84.20	20.32	37.42	48.41	57.09	63.73	18.96	33.28	42.45	49.14	54.85
LLBP	27.06	48.26	61.68	72.54	81.74	20.54	36.05	47.51	55.04	61.55	18.87	31.46	40.10	46.59	51.73
ULBP	25.91	47.68	61.52	72.50	81.17	20.02	35.62	46.49	54.03	61.07	18.25	30.55	39.05	45.48	50.90
LCVBP	32.33	55.81	70.46	79.90	87.71	**26.41**	44.25	55.59	63.77	70.18	**25.02**	**40.28**	49.55	56.31	61.49
WLD	33.09	56.14	71.03	80.58	87.12	26.36	43.61	53.88	61.82	68.22	24.07	39.21	48.57	55.20	60.84
QDWD	30.72	53.61	68.36	80.13	88.68	24.71	42.30	53.62	61.66	67.71	21.83	37.74	47.25	53.73	59.53
QIWD	**33.96**	**57.26**	**73.53**	**83.20**	**89.90**	25.93	**45.15**	**57.07**	**65.63**	**72.16**	22.91	40.22	**50.88**	**58.28**	**63.78**

2) Face Recognition: This experiment evaluates the performance of QWLD for face recognition using the NUST RWFR database. The following local descriptors are chosen for comparison, including WLD [30], LBP [45], LCVBP [46], robust LBP (RLBP) [48], completed LBP (CLBP) [49], and upper LBP (ULBP) and lower LBP (LLBP) [50]. For WLD, LBP, RLBP, CLBP, LLBP, and ULBP, the features are derived from each color components individually and concatenated together to get a final feature vector, while the LCVBP descriptor is extracted from the vector representation of the color images. Face recognition here is carried out as the person reidentification task in Section VI. Table IX shows the recognition results of all descriptors when the number of subjects N is set to 30, 60, and 90. We can find that LCVBP achieves the most satisfying performance among all LBP-based methods, and WLD obtains similar results as LCVBP. For QWLD descriptors, QDWD obtains close matching rates with WLD, and QIWD gains the best performance among all these methods.

D. Person Reidentification

In this experiment, the proposed QWLD is compared with several other local descriptors using all three person reidentification data sets. The local descriptors used in Section VII-C2 are also selected here. Besides, Zheng's method [35] and the histogram of oriented gradients (HOG) descriptor [51] are also considered. The HOG descriptor is extracted from all color channels as WLD- and the LBP-based methods. Zheng's method is designed for person reidentification, which extracts features from both the color and texture information of the original images.[6] The corresponding results are shown in Fig. 5.

Let us first see the experimental results on i-LIDS MCTS. The person number N is set to 30, 60, and 90, respectively. We can find that LCVBP, WLD, QDWD, and QIWD obtain better results than other methods on the whole. LCVBP and WLD achieve comparable performances when $N = 30$ and 60. As N increases to 90, the matching results of WLD are 2% higher than those of LCVBP. In this data set, QIWD leads to about 2%–3% than the second best method in most cases. When N is set to 60 and 90, QDWD achieves the second best results.

It is more challenging to reidentify the persons in the VIPER data set because it only contains two images for each person. We set N to 150, 300, and 450, respectively. In this data set, CLBP, Zheng's method, and QIWD achieve more satisfying performances, while RLBP obtains the worst results. In the situation of $N = 150$, the matching rates of CLBP, Zheng's method, and QIWD are comparable when r is equal to 1 and 2, while QIWD outperforms other methods as r is with larger values. If N increases to 300 and 450, QIWD obtains the best results when r is larger than 15.

The reidentification results on the ETHZ data set are finally given. Unlike VIPER, ETHZ contains about 58 images for per person. The person number N is set to 30, 60, and 90, respectively. In this test, LCVBP, WLD, QDWD, and QIWD are the best three methods, while RLBP and LLBP perform the worst. The results of LCVBP and WLD are quite similar and slightly better than QDWD. When r is set to 1 or 5, QIWD may exceed RLBP and LLBP by about 10%, and it obtains results comparable with LCVBP and WLD. When r increases, the matching rates of QIWD are superior to LCVBP and WLD by about 1% to 2% in all cases.

E. Time Complexity Analysis

Time complexity is an important aspect to evaluate a descriptor. In this section, we theoretically compare the computation cost of QWLD with LBP, WLD, and SIFT. Considering a color image with size of $M \times N$, the time complexities of LBP, WLD, and scale-invariant feature transform (SIFT) are as follows [30]:

$$O_{\text{LBP}} = \lambda_1 MN \tag{41}$$

$$O_{\text{WLD}} = \lambda_2 MN \tag{42}$$

$$O_{\text{SIFT}} \approx \lambda_3 (h_1 h_2)(g_1 g_2) MN \tag{43}$$

where λ_1, λ_2, and λ_3 are constants for the computation costs of each pixel in corresponding descriptor through additions, divisions, and filtering operations, respectively. h_1 and h_2 are the levels of octave and scales of each octave, respectively. g_1 and g_2 are the sizes of the convolution mask. Some improved LBP methods may have the same time complexities as LBP. Equations (41)–(43) indicate that LBP and WLD are more efficient than SIFT.

Compared with WLD, the main additional computation cost of QIWD lies in the calculation of the local differences
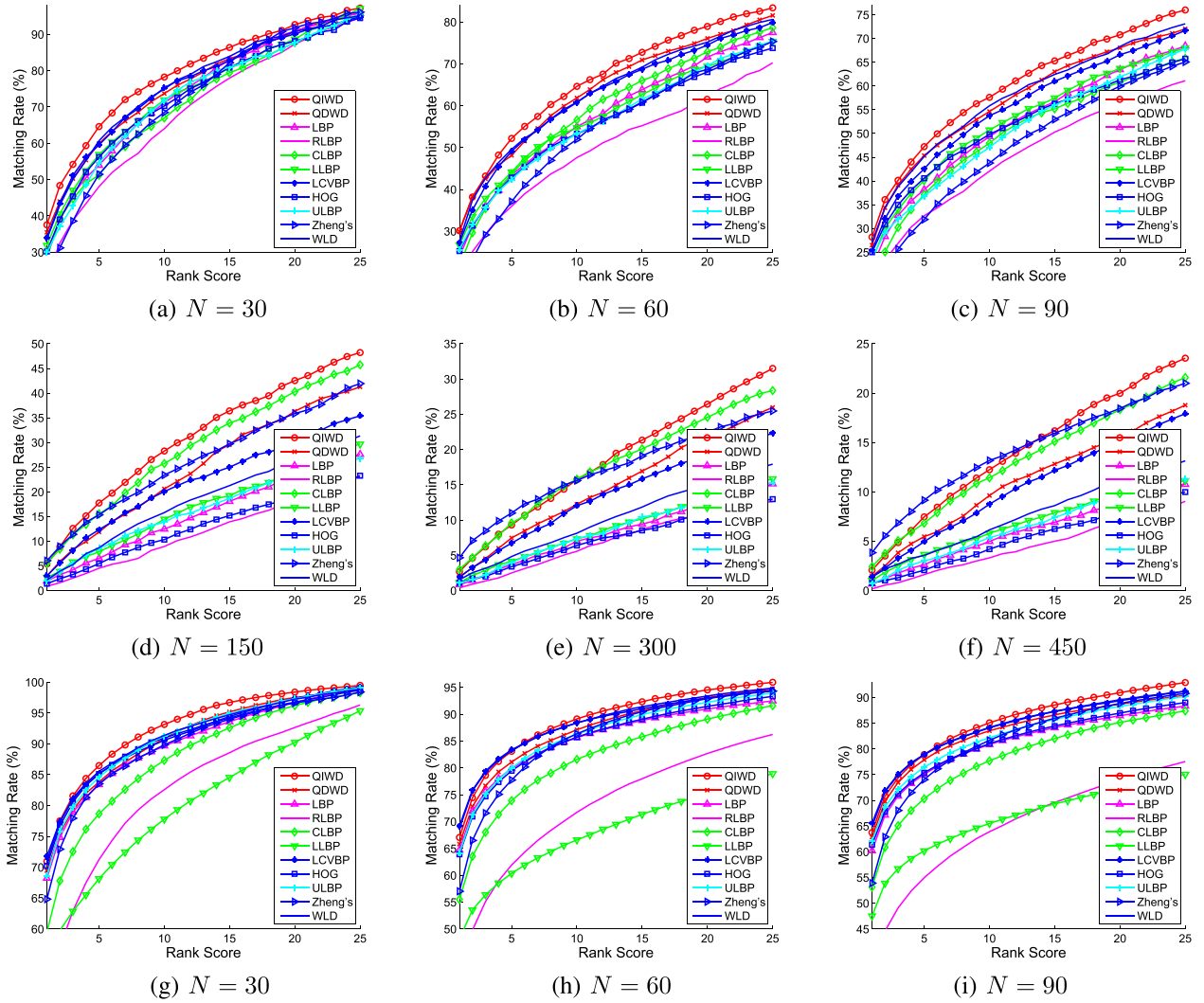
Fig. 5.   CMC results of different feature extraction methods on three used person reidentification data sets. (a)–(c) Results of i-LIDS MCTS. (d)–(f) Results of VIPER. (g)–(i) Results of ETHZ.

between the center pixel and its surrounding ones. This procedure is implemented by a convolution of a $z_1 * z_2$ template for a given image. In this paper, the size of template is set to 3×3 as in (30) and (34). Therefore, the time complexity of QIWD is as follows:

$$O_{\text{QIWD}} = \lambda_4(z_1 z_2) M N \tag{44}$$

where λ_4 is a constant and has the same meaning as the previous ones. For QDWD, if we directly calculate the QD by its definition, it will take a large computation cost. An alternative way is to simplify the calculation of the QD using the vector representation. For example, D_3 and D_5 are equivalent to (47) and (50). Hence, the time complexity of QDWD turns to

$$O_{\text{QDWD}} = \lambda_5 M N \tag{45}$$

where λ_5 is similar to the previous ones. Observing (41)–(45), we can find that QIWD takes larger time complexity than LBP and WLD, but it is more efficient than SIFT. Once the computation of QD is optimized, QDWD will achieve the similar time complexity as LBP and WLD.

VIII. CONCLUSION

In this paper, we proposed QWLD as a novel framework to derive local descriptors for color image feature extraction. QWLD is based on the QR of color images and WL. As a result, it contains the advantages of both QR and WL. Two quaternionic descriptors QDWD and QIWD were derived based on the QWLD framework. Experiments were carried out to evaluate the performances of the proposed quaternionic descriptors by different color image recognition problems, and the comparison results have shown the effectiveness of derived descriptors. To further improve the performance of QWLD, our future work will propose fast calculation algorithms for QDs, design more discriminative QDs for quaternions, and find suitable functions to describe the quaternionic increment.

APPENDIX
PROOF OF (13)

Proof: Rewrite $\dot{\mu}$, $\dot{\rho}$, $\dot{q}_1$, and $\dot{q}_2$ into the vector form as follows, respectively, $\dot{\mu} = (0, \boldsymbol{\mu}) = (0, (\sqrt{3}/3),$ $(\sqrt{3}/3), (\sqrt{3}/3))^T$, $\dot{\rho} = e^{(\pi/4)\dot{\mu}} = (\rho, \boldsymbol{\rho}) = ((\sqrt{2}/2),$ $(\sqrt{6}/6), (\sqrt{6}/6), (\sqrt{6}/6))^T$, $\dot{q}_1 = (0, \boldsymbol{q_1}) = (0, r_1, g_1, b_1)^T$,

and $\dot{q}_2 = (0, \boldsymbol{q_2}) = (0, r_2, g_2, b_2)^T$. Then $\dot{q}_1\dot{q}_2$ can be expressed by

$$\dot{q}_1\dot{q}_2 = (-\boldsymbol{q_1} \bullet \boldsymbol{q_2}, \boldsymbol{q_1} \times \boldsymbol{q_2}) = -\boldsymbol{q_1} \bullet \boldsymbol{q_2} + \boldsymbol{q_1} \times \boldsymbol{q_2} \quad (46)$$

where $\bullet$ and $\times$ denote the vector dot product and cross product, respectively.

According the definition of D_3 in (8) and (46), we have

$$\frac{1}{2}[(\dot{\rho}\dot{q}_1\dot{\rho}^* - \dot{\rho}^*\dot{q}_1\dot{\rho}) - (\dot{\rho}\dot{q}_2\dot{\rho}^* - \dot{\rho}^*\dot{q}_2\dot{\rho})]$$
$$= -2\rho(\boldsymbol{\rho} \times \boldsymbol{q_1}) + 2\rho(\boldsymbol{\rho} \times \boldsymbol{q_2}) = \boldsymbol{\mu} \times (\boldsymbol{q_2} - \boldsymbol{q_1})$$
$$= \frac{\sqrt{3}}{3} \begin{pmatrix} b_1 - b_2 - g_1 + g_2 \\ r_1 - r_2 - b_1 + b_2 \\ g_1 - g_2 - r_1 + r_2 \end{pmatrix} \triangleq \begin{pmatrix} r_4 \\ g_4 \\ b_4 \end{pmatrix}. \quad (47)$$

Similarly, (10) turns to

$$\boldsymbol{q_3} = 2(\boldsymbol{\mu} \bullet \boldsymbol{q_1})\boldsymbol{\mu} + (\boldsymbol{q_2} - \boldsymbol{q_1})$$
$$= \frac{1}{3} \begin{pmatrix} -r_1 + 2g_1 + 2b_1 + 3r_2 \\ 2r_1 - g_1 + 2b_2 + 3g_2 \\ 2r_1 + 2g_1 - b_1 + 3b_2 \end{pmatrix}. \quad (48)$$

Then

$$\frac{r_3 + g_3 + b_3}{3} = \frac{r_1 + g_1 + b_1 + r_2 + g_2 + b_2}{3}. \quad (49)$$

Rewriting D_5 into its vector form, it has the following:

$$\begin{pmatrix} r_3 \\ g_3 \\ b_3 \end{pmatrix} - \begin{pmatrix} \dfrac{r_3 + g_3 + b_3}{3} \\ \dfrac{r_3 + g_3 + b_3}{3} \\ \dfrac{r_3 + g_3 + b_3}{3} \end{pmatrix}$$
$$= \frac{1}{3} \begin{pmatrix} -2r_1 + g_1 + b_1 + 2r_2 - g_2 - b_2 \\ r_1 - 2g_1 + b_1 - r_2 + 2g_2 - b_2 \\ r_1 + g_1 - 2b_1 - r_2 - g_2 + 2b_2 \end{pmatrix} \triangleq \begin{pmatrix} r_5 \\ g_5 \\ b_5 \end{pmatrix}. \quad (50)$$

We can find that $r_4 \neq r_5$, $g_4 \neq g_5$, and $b_4 \neq b_5$, but they have the following relation:

$$\sqrt{r_4^2 + g_4^2 + b_4^2} = \sqrt{r_5^2 + g_5^2 + b_5^2}. \quad (51)$$

Now we derive the desired result in (13). ∎

REFERENCES

[1] W. R. Hamilton, *Elements of Quaternions*, W. E. Hamilton, Ed. London, U.K.: Longmans, Green, & Co., 1866.

[2] T. A. Ell and S. J. Sangwine, "Hypercomplex Fourier transforms of color images," *IEEE Trans. Image Process.*, vol. 16, no. 1, pp. 22–35, Jan. 2007.

[3] Ö. S. Subakan and B. C. Vemuri, "A quaternion framework for color image smoothing and segmentation," *Int. J. Comput. Vis.*, vol. 91, no. 3, pp. 233–250, 2011.

[4] L. Jin, H. Liu, X. Xu, and E. Song, "Quaternion-based impulse noise removal from color video sequences," *IEEE Trans. Circuits Syst. Video Technol.*, vol. 23, no. 5, pp. 741–755, May 2013.

[5] E. G. Karakasis, G. A. Papakostas, D. E. Koulouriotis, and V. D. Tourassis, "A unified methodology for computing accurate quaternion color moments and moment invariants," *IEEE Trans. Image Process.*, vol. 23, no. 2, pp. 596–611, Feb. 2014.

[6] S.-C. Pei and C.-M. Cheng, "Color image processing by using binary quaternion-moment-preserving thresholding technique," *IEEE Trans. Image Process.*, vol. 8, no. 5, pp. 614–628, May 1999.

[7] J.-C. Souyris and C. Tison, "Polarimetric analysis of bistatic SAR images from polar decomposition: A quaternion approach," *IEEE Trans. Geosci. Remote Sens.*, vol. 45, no. 9, pp. 2701–2714, Sep. 2007.

[8] P. Ginzberg and A. T. Walden, "Matrix-valued and quaternion wavelets," *IEEE Trans. Signal Process.*, vol. 61, no. 6, pp. 1357–1367, Mar. 2013.

[9] F. Shang and A. Hirose, "Quaternion neural-network-based PolSAR land classification in Poincare-sphere-parameter space," *IEEE Trans. Geosci. Remote Sens.*, vol. 52, no. 9, pp. 5693–5703, Sep. 2014.

[10] C. Jahanchahi and D. P. Mandic, "A class of quaternion Kalman filters," *IEEE Trans. Neural Netw. Learn. Syst.*, vol. 25, no. 3, pp. 533–544, Mar. 2014.

[11] Y. Xu, L. Yu, H. Xu, H. Zhang, and T. Nguyen, "Vector sparse representation of color image using quaternion matrix analysis," *IEEE Trans. Image Process.*, vol. 24, no. 4, pp. 1315–1329, Apr. 2015.

[12] B. Chen, H. Shu, H. Zhang, G. Chen, and L. Luo, "Color image analysis by quaternion Zernike moments," in *Proc. IEEE 20th Int. Conf. Pattern Recognit. (ICPR)*, Aug. 2010, pp. 625–628.

[13] B. J. Chen *et al.*, "Quaternion Zernike moments and their invariants for color image analysis and object recognition," *Signal Process.*, vol. 92, no. 2, pp. 308–318, 2012.

[14] L.-Q. Guo and M. Zhu, "Quaternion Fourier–Mellin moments for color images," *Pattern Recognit.*, vol. 44, no. 2, pp. 187–195, 2011.

[15] B. Chen, H. Shu, G. Coatrieux, G. Chen, X. Sun, and J. L. Coatrieux, "Color image analysis by quaternion-type moments," *J. Math. Imag. Vis.*, vol. 51, no. 1, pp. 124–144, 2015.

[16] J. Mennesson, C. Saint-Jean, and L. Mascarilla, "New geometric Fourier descriptors for color image recognition," in *Proc. 17th IEEE Int. Conf. Image Process. (ICIP)*, Sep. 2010, pp. 2685–2688.

[17] Z. Yang and S.-I. Kamata, "Hypercomplex polar Fourier analysis for color image," in *Proc. 18th IEEE Int. Conf. Image Process. (ICIP)*, Sep. 2011, pp. 2117–2120.

[18] L. Guo, M. Dai, and M. Zhu, "Quaternion moment and its invariants for color object classification," *Inf. Sci.*, vol. 273, pp. 132–143, Jul. 2014.

[19] D. G. Lowe, "Distinctive image features from scale-invariant keypoints," *Int. J. Comput. Vis.*, vol. 60, no. 2, pp. 91–110, 2004.

[20] H. Bay, T. Tuytelaars, and L. Van Gool, "SURF: Speeded up robust features," in *Proc. 9th Eur. Conf. Comput. Vis. (ECCV)*, 2006, pp. 404–417.

[21] D. Tao, X. Li, X. Wu, and S. J. Maybank, "General tensor discriminant analysis and Gabor features for gait recognition," *IEEE Trans. Pattern Anal. Mach. Intell.*, vol. 29, no. 10, pp. 1700–1715, Oct. 2007.

[22] Y. Wang, R. Hu, C. Liang, C. Zhang, and Q. Leng, "Camera compensation using a feature projection matrix for person reidentification," *IEEE Trans. Circuits Syst. Video Technol.*, vol. 24, no. 8, pp. 1350–1361, Aug. 2014.

[23] J. Jiang, X. Li, and G. Zhang, "SIFT hardware implementation for real-time image feature extraction," *IEEE Trans. Circuits Syst. Video Technol.*, vol. 24, no. 7, pp. 1209–1220, Jul. 2014.

[24] J.-M. Guo, H. Prasetyo, and J.-H. Chen, "Content-based image retrieval using error diffusion block truncation coding features," *IEEE Trans. Circuits Syst. Video Technol.*, vol. 25, no. 3, pp. 466–481, Mar. 2015.

[25] X. Wu and K. Kashino, "Second-order configuration of local features for geometrically stable image matching and retrieval," *IEEE Trans. Circuits Syst. Video Technol.*, vol. 25, no. 8, pp. 1395–1408, Aug. 2015.

[26] R. Lan, Y. Zhou, Y. Y. Tang, and C. L. P. Chen, "Person reidentification using quaternionic local binary pattern," in *Proc. IEEE Int. Conf. Multimedia Expo (ICME)*, Jul. 2014, pp. 1–6.

[27] J. Weeks, R. Lehoucq, and J.-P. Uzan, "Detecting topology in a nearly flat spherical universe," *Classical Quantum Gravity*, vol. 20, no. 8, p. 1529, 2003.

[28] A. K. Jain, *Fundamentals of Digital Image Processing*. Upper Saddle River, NJ, USA: Prentice-Hall, 1989.

[29] J. Chen, S. Shan, G. Chen, X. Chen, W. Gao, and M. Pietikainen, "A robust descriptor based on Weber's law," in *Proc. IEEE Conf. Comput. Vis. Pattern Recognit. (CVPR)*, Jun. 2008, pp. 1–7.

[30] J. Chen *et al.*, "WLD: A robust local image descriptor," *IEEE Trans. Pattern Anal. Mach. Intell.*, vol. 32, no. 9, pp. 1705–1720, Sep. 2010.

[31] B. Wang, W. Li, W. Yang, and Q. Liao, "Illumination normalization based on Weber's law with application to face recognition," *IEEE Signal Process. Lett.*, vol. 18, no. 8, pp. 462–465, Aug. 2011.

[32] C. Cai and S. K. Mitra, "A normalized color difference edge detector based on quaternion representation," in *Proc. IEEE Int. Conf. Image Process. (ICIP)*, Sep. 2000, pp. 816–819.

[33] X. Geng, X. Hu, and J. Xiao, "Quaternion switching filter for impulse noise reduction in color image," *Signal Process.*, vol. 92, no. 1, pp. 150–162, 2012.

[34] L. Jin and D. Li, "An efficient color-impulse detector and its application to color images," *IEEE Signal Process. Lett.*, vol. 14, no. 6, pp. 397–400, Jun. 2007.

[35] W.-S. Zheng, S. Gong, and T. Xiang, "Reidentification by relative distance comparison," *IEEE Trans. Pattern Anal. Mach. Intell.*, vol. 35, no. 3, pp. 653–668, Mar. 2013.

[36] A. Li, L. Liu, K. Wang, S. Liu, and S. Yan, "Clothing attributes assisted person reidentification," *IEEE Trans. Circuits Syst. Video Technol.*, vol. 25, no. 5, pp. 869–878, May 2015.

[37] United Kingdom Home Office. (2008). *Imagery Library for Intelligent Detection Systems (i-LIDS) Multiple Camera Tracking Scenario Definition*. [Online]. Available: http://www.homeoffice.gov.uk/science-research/hosdb/i-lids/

[38] W.-S. Zheng, S. Gong, and T. Xiang, "Associating groups of people," in *Proc. Brit. Mach. Vis. Conf.*, 2007, pp. 23.1–23.11.

[39] X. Wang, G. Doretto, T. Sebastian, J. Rittscher, and P. Tu, "Shape and appearance context modeling," in *Proc. IEEE 11th Int. Conf. Comput. Vis. (ICCV)*, Oct. 2007, pp. 1–8.

[40] B. Caputo, E. Hayman, and P. Mallikarjuna, "Class-specific material categorisation," in *Proc. 10th IEEE Int. Conf. Comput. Vis. (ICCV)*, Oct. 2005, pp. 1597–1604.

[41] J. Lu, J. Hu, X. Zhou, Y. Shang, Y.-P. Tan, and G. Wang, "Neighborhood repulsed metric learning for kinship verification," in *Proc. IEEE Conf. Comput. Vis. Pattern Recognit. (CVPR)*, Jun. 2012, pp. 2594–2601.

[42] J. Lu, X. Zhou, Y.-P. Tan, Y. Shang, and J. Zhou, "Neighborhood repulsed metric learning for kinship verification," *IEEE Trans. Pattern Anal. Mach. Intell.*, vol. 36, no. 2, pp. 331–345, Feb. 2014.

[43] A. Ess, B. Leibe, and L. Van Gool, "Depth and appearance for mobile scene analysis," in *Proc. IEEE 11th Int. Conf. Comput. Vis. (ICCV)*, Oct. 2007, pp. 1–8.

[44] D. Gray, S. Brennan, and H. Tao, "Evaluating appearance models for recognition, reacquisition, and tracking," in *Proc. IEEE Int. Workshop Perform. Eval. Tracking Surveill.*, Oct. 2007, pp. 41–47.

[45] T. Ojala, M. Pietikainen, and T. Maenpaa, "Multiresolution gray-scale and rotation invariant texture classification with local binary patterns," *IEEE Trans. Pattern Anal. Mach. Intell.*, vol. 24, no. 7, pp. 971–987, Jul. 2002.

[46] S. H. Lee, J. Y. Choi, Y. M. Ro, and K. N. Plataniotis, "Local color vector binary patterns from multichannel face images for face recognition," *IEEE Trans. Image Process.*, vol. 21, no. 4, pp. 2347–2353, Apr. 2012.

[47] A. Satpathy, X. Jiang, and H.-L. Eng, "LBP-based edge-texture features for object recognition," *IEEE Trans. Image Process.*, vol. 23, no. 5, pp. 1953–1964, May 2014.

[48] D. T. Nguyen, Z. Zong, P. Ogunbona, and W. Li, "Object detection using non-redundant local binary patterns," in *Proc. 17th IEEE Int. Conf. Image Process. (ICIP)*, Sep. 2010, pp. 4609–4612.

[49] Z. Guo, L. Zhang, and D. Zhang, "A completed modeling of local binary pattern operator for texture classification," *IEEE Trans. Image Process.*, vol. 19, no. 6, pp. 1657–1663, Jun. 2010.

[50] X. Tan and B. Triggs, "Enhanced local texture feature sets for face recognition under difficult lighting conditions," *IEEE Trans. Image Process.*, vol. 19, no. 6, pp. 1635–1650, Jun. 2010.

[51] N. Dalal and B. Triggs, "Histograms of oriented gradients for human detection," in *Proc. IEEE Comput. Soc. Conf. Comput. Vis. Pattern Recognit. (CVPR)*, Jun. 2005, pp. 886–893.
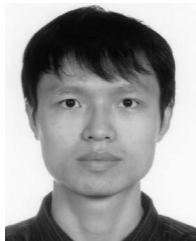
Rushi Lan received the B.S. and M.S. degrees from the Nanjing University of Information Science and Technology, Nanjing, China, in 2008 and 2011, respectively. He is currently pursuing the Ph.D. degree with the Department of Computer and Information Science, University of Macau, Macau, China.

His current research interests include image classification, image denoising, and metric learning.

Yicong Zhou (M'07–SM'14) received the B.S. degree from Hunan University, Changsha, China, in 1992, and the M.S. and Ph.D. degrees from Tufts University, Medford, MA, USA, in 2008 and 2010, respectively, all in electrical engineering.

He is currently an Assistant Professor with the Department of Computer and Information Science, University of Macau, Macau, China. His current research interests include multimedia security, image/signal processing, pattern recognition, and medical imaging.

Dr. Zhou is a member of the International Society for Photo-Optical Instrumentations Engineers and the Association for Computing Machinery. He received the third price of the Macau Natural Science Award in 2014.

Yuan Yan Tang (F'04) received the B.S. degree in electrical and computer engineering from Chongqing University, Chongqing, China, the M.S. degree in electrical engineering from the Beijing University of Post and Telecommunications, Beijing, China, and the Ph.D. degree in computer science from Concordia University, Montreal, QC, Canada.

He is currently a Chair Professor with the Faculty of Science and Technology, University of Macau, Macau, China, and a Professor/Adjunct Professor/Honorary Professor with several institutions, including Chongqing University, Concordia University, and Hong Kong Baptist University, Hong Kong. He has authored over 400 academic papers, and authored or co-authored over 25 monographs/books/book chapters. His current research interests include wavelets, pattern recognition, and image processing.

Dr. Tang is a fellow of the International Association for Pattern Recognition (IAPR). He is the Founder and Chair of the Pattern Recognition Committee of the IEEE International Conference on Systems, Man, and Cybernetics. He has served as the General Chair, the Program Chair, and a Committee Member of many international conferences. He is the Founder and General Chair of the series International Conferences on Wavelets Analysis and Pattern Recognition. He is the Founder and Chair of the Macau Branch of IAPR. He is the Founder and Editor-in-Chief of the *International Journal of Wavelets*, *Multiresolution*, and *Information Processing*, and an Associate Editor of several international journals.